

Microstructural characterization and corrosion behaviour of SLM CoCrMo alloy in simulated body fluid

M. Seyedi, F. Zanotto, E. Liverani, A. Fortunato, C. Monticelli, A. Balbo

CoCrMo base alloys are widely used for the production of orthopaedic implants because of their excellent mechanical properties and high corrosion resistance in biological fluids. However, despite the advances in this sector, untimely implant failures and dissatisfaction are still observed in patients. The fabrication of customized implants by Selective Laser Melting should permit to overcome some common problems, like mismatch between the joint prosthesis and the natural joint conformation, non-physiological load transfer and scarce osteointegration. However, some parameters related to the process optimization in terms of final density and mechanical properties are critical and the evaluation of their influence on corrosion resistance of the components is reputed fundamental. In this work SLM technique was used to produce two types of samples based on ASTM F1527 CoCrMo alloy by using different process parameters. The corrosion behaviour of the two materials was investigated by recording the EIS spectra and the polarization curves during 15 days of immersion in Phosphate-Buffered Saline (PBS) solutions at pH 7.4. The samples showed a fine microstructure, characterized by Mo enrichment at the cell boundaries. Both types of samples showed low corrosion rates in the studied environments because of the formation of a very protective oxide film on the sample surfaces with high resistance to localized corrosion, but the finer microstructure ensured slightly higher corrosion resistance.

KEYWORDS: BIOMATERIALS, SELECTIVE LASER MELTING, CoCrMo ALLOYS, CORROSION, SIMULATED BODY FLUIDS

INTRODUCTION

Traditional endoprostheses are widely used to replace joint surfaces damaged by severe trauma or degenerative articular disease. Typical metallic biomaterials used to fabricate implant devices include austenitic stainless steels, Co-Cr and Ti alloys. In particular, the use of high-strength Co-Cr based alloys for improving the durability of such devices has attracted much attention in the past years because of their excellent properties, including high mechanical strength, good biocompatibility, high wear and corrosion resistance [1-3]. Although these materials have been used successfully for over 5 decades, in the case of some specific joint types frequent failures and patients' dissatisfaction have been reported [4]. The reasons for these failures were related to a number of factors, such as: limited availability of prosthesis size and shape, difference in mechanical properties between bone and implant materials, unsatisfactory osteointegration and foreign body reaction induced by inflammatory cells [4-6]. Selective laser melting (SLM) is a very promising technique that can overcome some of these issues. In fact, this technique allows obtaining completely customizable and scalable prostheses with complex shapes, through the consolidation of metal powders layer by layer. It is, therefore, possible to control the microstructure characteristics of the product and to manufacture dense components, porous graded or fully customized architectures, improving oste-

ointegration and bone adaptation [7-9]. Biofunctionality and biocompatibility are fundamentals factors for the selection of biomaterial alloys and the corrosion resistance of metal implants in the body fluids is closely related to their biocompatibility [1]. Recently, the potential of using SLM materials was investigated in vitro for dental applications [9,10]. The materials fabricated with SLM technology seem to be promising in terms of corrosion resistance, but their behavior in biological environments has not been studied

**Mahla Seyedi, Federica Zanotto,
Cecilia Monticelli, Andrea Balbo**

Corrosion and Metallurgy Study Centre "A. Daccò", University of Ferrara, Department of Engineering, via Saragat 4a, Ferrara, Italy

Erica Liverani, Alessandro Fortunato

University of Bologna, Department of Industrial Engineering, viale Risorgimento 2, Bologna, Italy

Additive manufacturing

in depth. In a previous work [11], a proper selection of different laser process parameters, bulk and surface fabrication was optimized in terms of mechanical properties. In this work, the same strategy was adopted to fabricate two different types of samples and the corrosion behaviour of the CoCrMo alloy was investigated in solutions simulating biological fluids.

EXPERIMENTAL

The studied materials were prepared with SLM technique starting from a commercial powder of CoCrMo alloy (LPW Technology Ltd, Runcorn Cheshire, UK) whose composition meets the standard ASTM F1537. Tab. 1 reports the composition of the raw powder. The samples were fabricated with a SISMA MYSINT100 system (Sisma, Piovene Roccheta, Italy) by using two different sets of parameters, as indicated in tab. 2. The hatch distance (space between two adjacent laser tracks) was maintained constant to the value of 0.06 mm and a chessboard laser scan strategy was adopted. All materials were characterized by a scanning electron microscope (SEM, Zeiss MA15/LaB6) coupled with an energy dispersive spectroscopy (EDS) system (X-Act/INCA, Oxford Instruments) and by X ray diffraction technique (Bruker D8 advances Billerica USA).

The biological environment was simulated by using a phos-

phate buffered saline (PBS) solution at pH=7.4, whose composition is shown in tab. 3. All samples were exposed to the solutions that simulated body fluids (SBF) for 15 days at the temperature of $37\pm 1^\circ\text{C}$. Electrochemical impedance spectroscopy (EIS) was used to monitor the evolution of the corrosion behaviour during the immersion period. The spectra were collected at the corrosion potential (E_{cor}) by imposing a $10\text{ mV}_{\text{rms}}$ amplitude excitation voltage in the frequency range $10^4 - 10^{-3}\text{ Hz}$, and by taking five measurements per decade. From each spectrum the polarization resistance (R_p) value was estimated as the limit of the real part of the impedance at frequency tending to 0. At the end of tests the polarizations curves (PC) were recorded at a scan rate of 0.1 mV s^{-1} . Preliminary cyclic voltammetry (CV) tests were also conducted, in order to better investigate the electrochemical behaviour of the two different sample types. Each CV test consisted in 5 cycles recorded at a sweep rate of 120 mV s^{-1} in the potential ranges $(-1.5 \div +0.7)\text{ V}_{\text{SCE}}$ and $(-0.25 \div +0.7)\text{ V}_{\text{SCE}}$. Before each test, the samples were polarized at $-1.5\text{ V}_{\text{SCE}}$ for 80 s. The electrochemical tests were performed with a PAR 2263 potentiostat/FRA/galvanostat (EIS), and with a PAR 273A potentiostat/galvanostat (PC and CV).

Tab. 1 - EDS analysis of CoCrMo powders chemical composition (wt%)

C	N	Al	Si	Cr	Mn	Fe	Co	Ni	Mo	La
≤ 0.04	nd	nd	0.77 ± 0.05	28.06 ± 0.33	0.68 ± 0.11	0.12 ± 0.01	64.23 ± 0.16	nd	5.92 ± 0.11	0.07 ± 0.03

Tab. 2 - Process parameters used and obtained relative densities.

Test	Power (W)	Scan speed (mm/s)	Fluence (J/mm^3)	Relative density (%)
B1	150	900	138.8	99.8
B2	90	1200	53.6	95

Tab. 3 - Composition, electrical conductivity and pH of simulated body fluid (SBF) solution

Na_2HPO_4 (g/L)	KH_2PO_4 (g/L)	KCl (g/L)	NaCl (g/L)	Total Cl ⁻ (M)	\wedge ($\mu\text{S}/\text{cm}$)	pH
1.42	0.245	0.2	8.8	0.15	17.15	7.4

RESULTS AND DISCUSSION

The adopted laser parameters (tab. 2) induced different microstructural characteristics in the fabricated materials. High fluence processes promoted powder melting instead of sintering, so enabling the production of denser materials. In fact, the sample B1, obtained under high fluence conditions, showed a high relative density (99.85 %) and a low level of residual porosity, instead the B2 samples, obtained with low fluence process, were characterized by a lower relative density (95%) with respect to the B1 and by a microstructure with some large pores (up to 200 μ m). The microstructure of the produced samples is shown in fig 1. In both cases, the SEM observation highlighted a fine and elongated cellular microstructure formed within the melt pool. In fact, during the SLM process the alloys undergo a rapid heating, through the laser scan, followed by a very rapid cooling that produces an undercoo-

led melt. These high solidification rates and high level of non-equilibrium conditions induced the development of a microcellular structure and suppressed the formation of micro-sized carbides. Fig. 1 clearly shows a difference in the size of the microcells in the two samples: the sample B1 (fig. 1a) was characterized by coarser microcells with respect to the sample B2 (fig. 1b). This difference is probably due to the higher laser scanning speed and lower laser power (lower fluence) used for B2, which promoted a cell size refinement, due to a shorter persistence at high temperature during the layer build up. An elemental profile analysis carried out by SEM/EDS through these microstructural features on B1 sample, revealed clear Mo enrichment and Co depletion localized at the cell boundaries. Similar effects were observed on B2 sample.

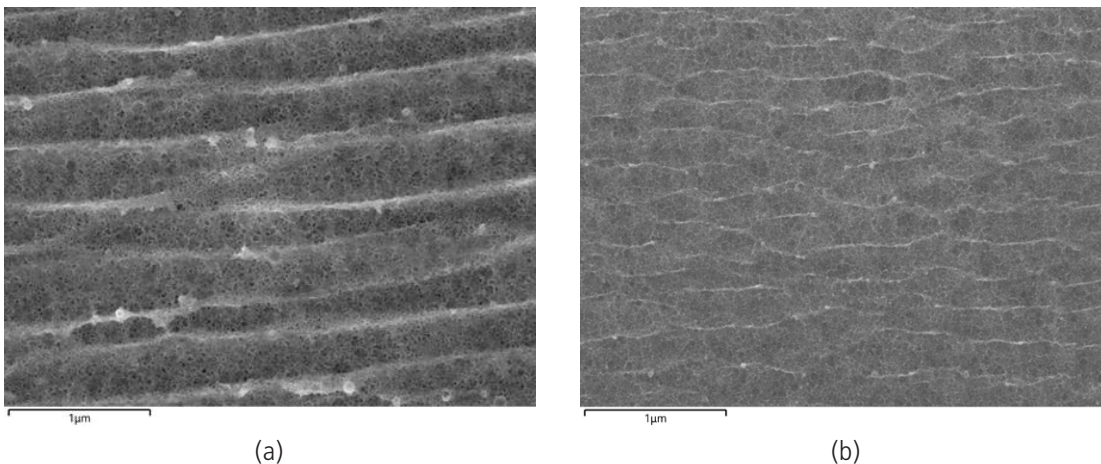


Fig. 1 - SEM image of the microstructures of (a) B1 and (b) B2 samples after electrolytic etching.

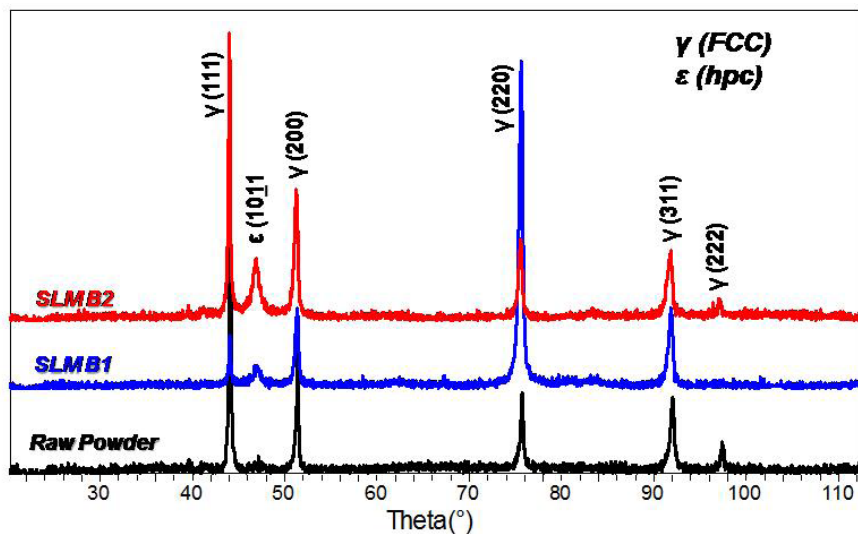


Fig. 2 - XRD diffraction pattern of raw powder, B1 and B2 specimens.

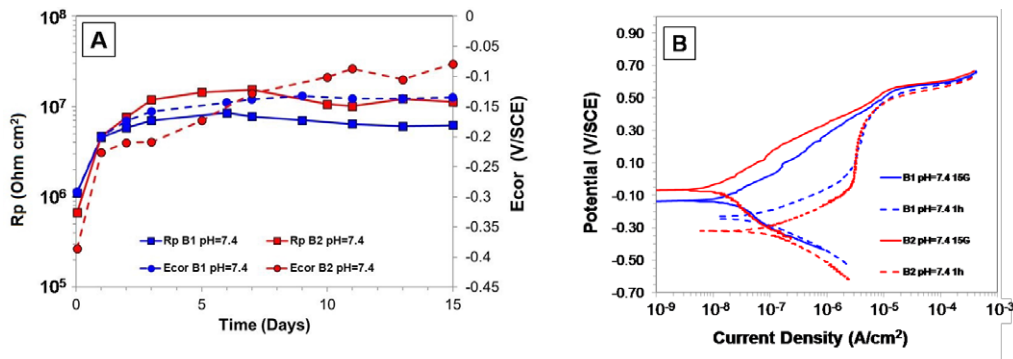


Fig. 3 - A) R_p and E_{cor} values and B) polarization curves recorded during the exposure to SBF.

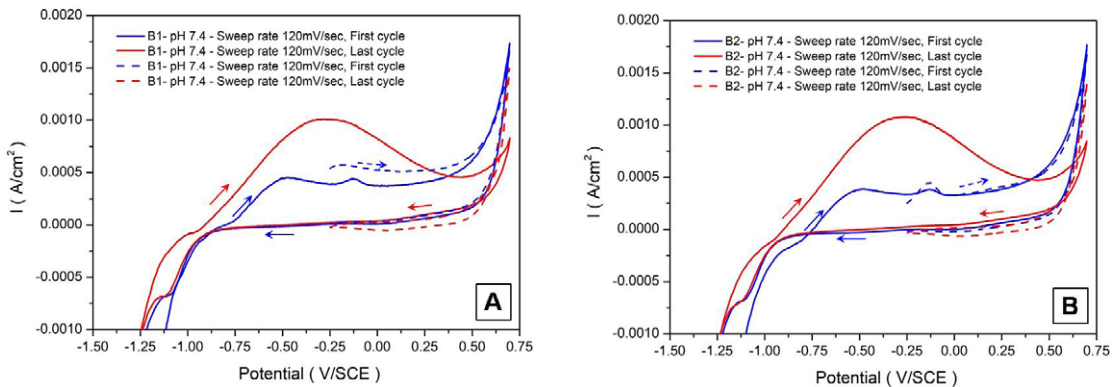


Fig. 4 - Cyclic voltammograms recorded on SLM samples in SBF at 120 mVs^{-1} . A) B1; B) B2.

Fig. 2 shows the XRD patterns obtained from the starting powder and from B1 and B2 samples, under spinning conditions. The XRD analysis showed that in all cases the metastable fcc phase (γ phase) is mainly retained at room temperature as the martensitic transformation from the metastable fcc to hcp phase (ϵ phase) is hindered during fast cooling below T_c (martensitic transformation critical temperature), such as during air cooling [12]. However, some amounts of ϵ phase were detected on both SLM samples (fig. 2, peak at 46.5°) since the transformation $\gamma \rightarrow \epsilon$ partially occurred during each new layer build up, due to heating of the sample sublayers at temperatures below T_c . The data indicated a higher amount of this phase in the B2 samples with respect to both B1 and raw powder, suggesting that, during each new layer deposition in B2 samples, the lower laser fluence induced the achievement of lower temperatures in comparison to those present on B1, so permitting a higher degree of martensitic transformation [9].

The corrosion behaviour of the SLM alloys was studied by monitoring the R_p values of both sample types, during

15 days of exposure to the selected SBF. The R_p and E_{cor} values are shown in fig. 3a. After 1 hour immersion in PBS at pH= 7.4, on B1 sample R_p values of $1\text{ M}\Omega\text{ cm}^2$ were detected, while B2 showed lower values, close to $0.7\text{ M}\Omega\text{ cm}^2$. For both B1 and B2 samples, R_p values increased rapidly during the first immersion period (1-3 days), with B2 samples always exhibiting higher R_p values, till the end of the immersion period. The corresponding E_{cor} values increased during the first days of exposure on both samples and then, in the case of B1 sample they settled at about -0.140 V_{SCE} , until the end of exposure, while on B2 they continuously increased up to -0.080 V_{SCE} . These results suggested that the air-formed oxide films on the alloys continuously improved their protectiveness particularly on B2.

The polarization curves collected after 1 hour and at the end of exposure period are shown in fig. 3b. At short immersion time, both B1 and B2 showed a passive behaviour and low corrosion currents (i_{cor}) around 9×10^{-8} and 10^{-7} A/cm^2 for B1 and B2 sample respectively. However, after 15 days of immersion, the anodic currents

significantly decreased, particularly on B2, inducing an ennobling of E_{cor} and a reduction of i_{cor} down to 2×10^{-8} A/cm² for B1 and 9×10^{-9} A/cm² for B2 sample. These results confirmed that at the end of the exposure B2 exhibited a higher corrosion resistance in comparison to B1, as highlighted by EIS measurements. At around $+0.57 V_{SCE}$ a rapid increase in the anodic current densities was measured. At these noble potential values both water oxidation and transpassive dissolution may occur [13, 16], but no pitting attack was observed by accurate SEM observations.

Fig. 4 collects the first and the fifth (the last) cycle of the CV tests carried out on B1 and B2 samples, at a sweep rate of 120 mV s^{-1} , in the two investigated potential ranges. B1 and B2 samples exhibited similar voltammograms. In the potential range from $-1.5 V_{SCE}$ to $0.7 V_{SCE}$, the direct scan of the first cycle (solid blue line) showed initially very high cathodic currents which are likely the sum of multiple reduction reactions (water and oxygen reduction and also surface oxide reduction if oxides are still present after pre-conditioning at $-1.5 V_{SCE}$). Then, an anodic peak at $-0.5 V_{SCE}$ is detected, related to electroformation of Co(II) hydroxide from Co metal [17] and a second peak is visible at $-0.125 V_{SCE}$, likely related to further oxidation of Mo oxides [18]. In the range $+0.6 \div +0.7 V_{SCE}$, compatible with both water oxidation and transpassive Cr dissolution, anodic currents increase significantly. During the reverse scan, the peak corresponding to Co(II) hydroxide reduction to Co metal is detected at about $-1.1 V_{SCE}$ [17]. In the subsequent cycles, an increase in anodic currents was observed in the potential range between the two previously quoted anodic peaks (-0.5 and $-0.125 V_{SCE}$) and in the last cycle (solid red line) only a broad anodic peak centred at $-0.25 V_{SCE}$ was detected. In the CV test performed in the potential range from $-0.25 V_{SCE}$ to $+0.7 V_{SCE}$, the peak at $-0.125 V_{SCE}$ was again detected in the first anodic cycle (blue dashed line), suggesting that this peak is not due to further oxidation of the species produced by oxidation at $-0.5 V_{SCE}$. On cycling (last cycle: red dashed line), the anodic current decreased progressively, showing that if the potential range permitting the oxide

layer reduction is not reached, a more and more protective surface film forms. This also suggests that in the range $+0.6 \div +0.7 V_{SCE}$ negligible transpassivity occurs because cycling including these high anodic potentials does not impair the oxide film protectiveness.

The results obtained showed that the process parameters adopted for the production of the samples have important effects on both the microstructural characteristics and the corrosion behavior. The B2 samples fabricated with the low-fluence process displayed some porosity and a refinement of the microstructure due to a shorter persistence at high temperature during the layer build up. As pointed out by both EIS measurements and PC tests, these B2 samples exhibited a better corrosion behaviour with respect to B1 after long immersion times, in neutral PBS solution. It is likely that in the presence of a finer microstructure, lower levels of Mo micro-segregation occur, so inducing a stronger and more uniform passivity. The porosity present on B2 does not affect its corrosion behaviour. Preliminary results obtained with CV tests, clearly stress the high stability of the surface passive film, which is maintained at high anodic potentials if the cathodic potential range allowing for oxide film reduction is avoided.

CONCLUSIONS

- The selected SLM parameters allow to obtain samples with different microstructural characteristics: B2 sample has a higher porosity than B1 but a finer cellular microstructure.
- Samples obtained with SLM technique show low corrosion rates in the tested environment that decrease during the exposure. The porosity present in the B2 does not affect the corrosion behaviour;
- The process parameters affect the corrosion behaviour: sample B2 has lower corrosion rates than sample B1 in all tested conditions;
- Lower levels of Mo micro-segregation on the cells boundary in the samples B2 allow for a more uniform Mo distribution in the passive film making it more protective.

Additive manufacturing

REFERENCE

- [1] Chen Q, Thouas GA, *Mat. Sci. Eng. R.* 87 (2015) 1–57.
- [2] Takayuki N et al., *Advance in Metallic Biomaterials, Tissue, Materials and Biological Reaction*. 1st ed. Springer-Verlag Berlin Heidelberg; 2015.
- [3] Niinomi M, *Sci. Technol. Adv. Mater.*, 4 (2003) 445-454.
- [4] Gougoulias N, Khanna A, Maffulli N, *Clin. Orthop Relat R*, 468 (2010) 199-208.
- [5] Gilbert JL, Sivan S, Liu Y, Kocagöz SB, Arnholt CM, Kurtz SM, *J. Biomed Mat Res.*, 130A (2015) 211-217.
- [6] Anderson JM, A. Rodriguez A, Chag DT, *Semin. Immunol.*; 20, (2008) 86-100.
- [7] Xin XZ, Chen J, Xiang N, Wei B, *Cell Biochem. Biophys.*, 67 (2013) 983-990.
- [8] Gu DD, Meiner W, Wissenbach K, Poprawe R. *Inter. Mat Rev. a* 57 (2012) 133-166.
- [9] Hedberg YS, Quian B, Schen Z, Virtanen S, Wallinder IO, *Dental Materials*; 30 (2014) 525-534.
- [10] Lu Y, Wu S, Gan Y, Li J, Zhao C, Zhuo D, Lin J, *Mat. Sci. Eng: C*, 49 (2015) 517-525.
- [11] Liverani E, Fortunato A, Leardini A, Belvedere C, Siegler S, Ceschini L, Ascari A, *Mat&Des.* 106 (2016) 60-68.
- [12] Lopez HF, Saldivar-Garcia AJ, *Metall. Trans. A.* 39 (2008) 8-18.
- [13] Bettini E, Eriksson T, Boström M, Leygraf C, Pan J, *Electro. Acta* 56 (2011) 9413-9419.
- [14] Bettini E, Boström M, Leygraf C, Pan J, Nature of Current Increase for a CoCrMo Alloy. "transpassive" Dissolution vs. Water Oxidation *Int. J. Electrochem. Sci.* 8 (2013) 11791-11804.
- [15] Vidal VC, Muñoz AL. *Corros. Sci.* 50 (2008) 1954-1961.
- [16] Hodgson AWE, Kurz S, Virtanen S, Fervel V, Olsson C-OA, Mischler S. *Electro. Acta*; 49 (2004) 2167-2178.
- [17] Metikos-Hukovic MR, Babic R, *Corros. Sci* 49 (2007) 3570-3579.
- [18] Metikos-Hukovic MR, Pilic Z, R. Babic R, Omanovic D. *Acta Biomater.* 2 (2006) 693-700.